Journal of Chromatography, 467 (1989) 341–356
Elsevier Science Publishers B.V., Amsterdam — Printed in The Netherlands

CHROM. 21 318

HIGH-SPEED SIZE CHARACTERIZATION OF CHROMATOGRAPHIC SILICA BY FLOW/HYPERLAYER FIELD-FLOW FRACTIONATION

S. KIM RATANATHANAWONGS and J. CALVIN GIDDINGS*
Department of Chemistry, Henry Eyring Building, University of Utah, Salt Lake City, UT 84112 (U.S.A.)
(Received December 6th, 1988)

SUMMARY

Flow/hyperlayer field-flow fractionation (FFF) has been successfully applied to the rapid size-based fractionation and characterization of various 3-μm and 5-μm commercial high-performance liquid chromatography silica supports. Because high-resolution information on both average particle diameter and size distribution was obtained in less than 3 min by using a relatively simple apparatus, the method is attractive for the routine characterization of chromatographic packing material. Flow/hyperlayer FFF is not only faster than most sedimentation methods, it is ideally suited for the characterization of porous particles since separation is based solely on diameter and is independent of density.

INTRODUCTION

The column is often referred to as the heart of the chromatographic system. However, the physical characteristics of the packing material on which the chromatographic activity of the column is based are often not well defined. The uncertainties that exist involve differences between nominal and actual mean particle diameters, the breadth of size distributions, batch-to-batch size variations, and the presence of fines and particle agglomerates, to name a few[1–5]. These factors result in inconsistent column-to-column performance and in some cases high back pressures. The inaccuracy in the reported characteristics of column packings could present a problem in the correlation of experimental results from different columns. In particular, these inaccuracies could interfere with the correlation of column performance according to reduced plate height/reduced flow velocity parameters, as first proposed by one of the authors[6]. Thus, it is of importance to gain as much accurate information as possible concerning the physical properties of the column packing material.

Many of the methods that have been used for the size-based separation and for the determination of mean particle diameters and size distributions of chromatographic supports are based on sedimentation. McMurtrey and DesLauriers[7], for example, employed sedimentation under gravity for the preparative-scale fractionation of thin-layer chromatography silica. The resulting material gave a comparable performance to commercial high-performance liquid chromatography (HPLC) pack-

0021-9673/89/$03.50

ing materials. However, the sedimentation process was time consuming, requiring up to 12 h for 5-μm particles. Unger and Gimpel[8] reported an analysis time of only 30 min for the size determination of 10-μm silica using photosedimentation. However, this analysis time did not include the time needed for measurement of the specific pore volume and the apparent density of the porous silica particles, parameters used in the subsequent calculation of the Stokes diameter. The diameters obtained by photosedimentation differed from those of scanning electron microscopy by up to 12%. Large discrepancies were observed for particles with big pores (*e.g.*, 400 nm). In a related work, Hanggi and Carr[9] monitored the turbidity of a settling silica suspension at a specific observation plane. Particle size distributions and mean particle diameters were derived from the resulting absorbance *versus* time curve using an assumed density for solvent-filled silica. Analysis times were of the order of 2 h for 5-μm silica.

Another process utilizing gravitational sedimentation forces, but in this case falling in the field-flow fractionation (FFF) category, was described by Giddings *et al.*[10]. These authors used sedimentation/steric FFF to examine a number of different chromatographic supports with regard to their size characteristics. Analysis times were under 30 min for silica particles of diameters between 5 and 20 μm. More recently, using a centrifuge in place of gravity, run times were reduced to 3–4 min[11], but this modified FFF technique has not been applied to chromatographic supports. A comparison of the system used in this work, flow/hyperlayer FFF, and all the techniques using sedimentation will be made in a later section.

Other methods that have been used for the determination of the particle size distribution of porous silicas include microscopy[1,8] and electrozone sensing[2,12,13]. Column permeability has also been used as a means by which the average particle diameter of the column packing can be approximated[2,14]. For a general discussion on porous silica sizing methods, see ref. 15.

FFF was first proposed and implemented in the latter half of the 1960s. Since then it has evolved into a versatile family of methods with many subtechniques, each applicable to a different class of macromolecules and particulate materials. These subtechniques are categorized by the type of field employed and the mode of operation. A discussion of the nomenclature and a description of the various subtechniques is given by Giddings *et al.*[16].

Generally, FFF utilizes laminar flow in a channel formed between two closely spaced parallel plates across which a driving force is applied. The FFF process can be carried out in many ways and applied to many materials. Of the subtechniques available, both sedimentation/steric and flow/hyperlayer FFF are applicable to large (>1 μm diameter) particles. In both cases, sample is injected into the FFF channel followed by a stopflow period during which the driving force remains operational. The particles are positively displaced by the driving force to form a thin layer near the so-called accumulation wall. When the channel flow is restarted, particles of different diameters are transported downstream at different rates depending on the degree of their protrusion into the parabolic flow profile. In both methods the centers of mass of the larger particles occupy faster streamlines; thus, they elute more quickly than the smaller particles.

In the steric mode of operation, particles migrate very close to the accumulation wall. Discrepancies between the predicted and experimental retention ratios that have

been observed[10,17] are due to hydrodynamic lift forces which tend to drive the particles away from the accumulation wall. With sufficiently strong lift forces, the particles form a narrow band, or hyperlayer, at some distance above the accumulation wall. This gives us hyperlayer FFF[18].

Because the particles in hyperlayer FFF occupy faster flowing streamlines than they would near the wall, they elute more quickly than predicted by the steric model. The position of the compressed particle cloud within the channel corresponds to the point at which the two opposing forces, the primary driving force (in the present case caused by crossflow) and the lift force, are balanced. Retention in flow/hyperlayer FFF is thus based on the relationship between the crossflow driving force and the lift force. The latter force is a complex function of channel flow velocity, particle diameter, and distance from the wall. The lift force, which becomes increasingly significant at high flow-rates and for large particles, is currently being investigated[19].

THEORY

The parabolic flow profile in an FFF channel is described by the equation

$$v = 6\langle v\rangle \left[\frac{x}{w} - \left(\frac{x}{w}\right)^2\right] \tag{1}$$

where v is the local fluid velocity, $\langle v\rangle$ is the mean flow velocity, x is the distance from the accumulation wall, and w is the channel thickness. As previously noted, the balance between two opposing forces establishes an equilibrium position, $x = x_{eq}$, for each particle band in the channel. A band at position x_{eq} is carried along at a velocity v defined by the above parabolic equation.

The retention ratio R is defined as $v/\langle v\rangle$. From eqn. 1 we obtain the following expression for R[18]

$$R = \frac{v}{\langle v\rangle} = 6\left[\frac{x_{eq}}{w} - \left(\frac{x_{eq}}{w}\right)^2\right] \tag{2}$$

Because x_{eq} depends in part on imperfectly characterized lift forces, the positions of the particle bands in the channel cannot be accurately predicted. Hence the particle velocities v and retention ratios R are not presently calculable from first principles. This inability to predict retention ratios in this size range necessitates the use of calibration curves from which the diameter of different fractions can be obtained. Fortunately, in the size range of chromatographic supports, excellent latex particle standards of precisely known diameters are available for calibration.

The calibration process is best understood in relationship to selectivity. The diameter-based selectivity, which represents the intrinsic resolving power of the system with respect to particle diameter d, is defined as[20]

$$S_d = \left|\frac{\mathrm{d}\log t_r}{\mathrm{d}\log d}\right| \tag{3}$$

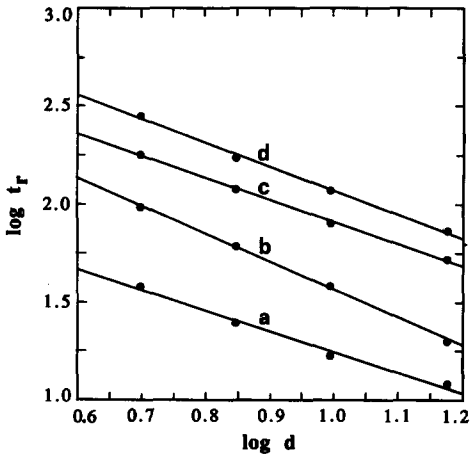

Fig. 1. Calibration curves of log retention time *versus* log diameter under different separation conditions. (a) Channel flow-rate, $\dot{V} = 7.55$ ml/min, crossflow flow-rate, $\dot{V}_c = 1.70$ ml/min; (b) $\dot{V} = 6.34$ ml/min, $\dot{V}_c = 2.09$ ml/min; (c) $\dot{V} = 3.64$ ml/min, $\dot{V}_c = 2.04$ ml/min; and (d) $\dot{V} = 3.93$ ml/min, $\dot{V}_c = 3.33$ ml/min. The latex particle standards used to establish the calibration curves have nominal diameters of 15.00, 9.87, 7.0 and 5.002 μm. The slope of the calibration curves yields the S_d value needed in polydispersity calculations.

where t_r is the particle retention time. Both theoretical and empirical evidence suggests that S_d is nearly constant over a substantial range of diameters for most FFF systems[21,22]. Thus a plot of log d *versus* log t_r generally yields a straight line. By injecting latex standards of different diameters and plotting log t_r against log d, a value for S_d may be obtained from the slope of the line. Such plots can be used for calibration purposes. Fig. 1 shows a series of selectivity plots or calibration curves for different diameter latex particle standards fractionated using various separation conditions. These graphs can be used to obtain particle diameters from the measured elution times of the samples. The different positions of the calibration lines in Fig. 1 reflect the complex interplay between lift forces and crossflow and channel flow-rates.

As in chromatography, peak broadening in FFF is measured by plate height H. For large particles, where axial diffusion can be assumed to be negligible, H can be written as the sum of a system contribution H_s and a sample polydispersity contribution H_p

$$H = H_s + H_p \tag{4}$$

Most particulate samples, including chromatographic supports, have considerable size variation (> 50% between size extremes). Because of the high selectivity ($S_d > 1$) of the system as displayed by Fig. 1, the different particle sizes are well spread out along the retention time axis t_r (see later), yielding a large effective plate height H_p. Generally we can assume $H_p \gg H_s$; the observed plate height H can thus be approximated as

$$H \cong H_p \tag{5}$$

The polydispersity of particulate samples is often expressed in terms of the

coefficient of variation (C.V.), equal to the standard deviation in particle diameter σ_d divided by the mean diameter d. The following expression, yielding C.V. in terms of experimentally observed elution profiles, is based on a previous derivation[23] that leads to

$$H_p = LS_d^2\left(\frac{\sigma_d}{d}\right)^2 = LS_d^2(\text{C.V.})^2 \tag{6}$$

which shows H_p to be dependent on the channel length L, the selectivity S_d, and the coefficient of variation (C.V.). Assuming that the polydispersity is the only significant contributor to the plate height (see eqn. 5) and expressing the number N of theoretical plates as L/H, we get

$$N = \frac{L}{H_p} = \frac{1}{S_d^2(\text{C.V.})^2} \tag{7}$$

Eqn. 7 can be rearranged in the following manner

$$\text{C.V.} = \frac{1}{S_d\sqrt{N}} \tag{8}$$

to yield C.V. in terms of measured plate numbers. Alternatively, if we express N as

$$N = \left(\frac{t_r}{\sigma_t}\right)^2 \tag{9}$$

where σ_t is the peak standard deviation in units of time, we obtain

$$\text{C.V.} = \frac{\sigma_t}{S_d t_r} \tag{10}$$

which relates C.V. directly to the experimental quantities σ_t and t_r. The variables in the above equation for C.V. are measured from the fractograms.

EXPERIMENTAL

Equipment

The modules that comprise the flow FFF system used here for hyperlayer operation are shown in Fig. 2. A standard HPLC pump, Kontron 410 (Kontron Electrolab, London, U.K.) is used to provide the axial channel flow while a syringe pump (designed in-lab) delivers a continuous and pulseless flow of carrier liquid across the channel. The Spectroflow 757 UV–visible detector (Applied Biosystems, Ramsey, NJ, U.S.A.) was set at 254 nm and in most cases 0.02 a.u.f.s. Short time constants (0.1–1 s) were used so as not to bias the shape of the response, particularly for high-speed runs. Coiled lengths of 0.01 in. (254 μm) internal diameter stainless-steel tubing were used to balance the flow-rates of the crossflow and channel flow. Pressure

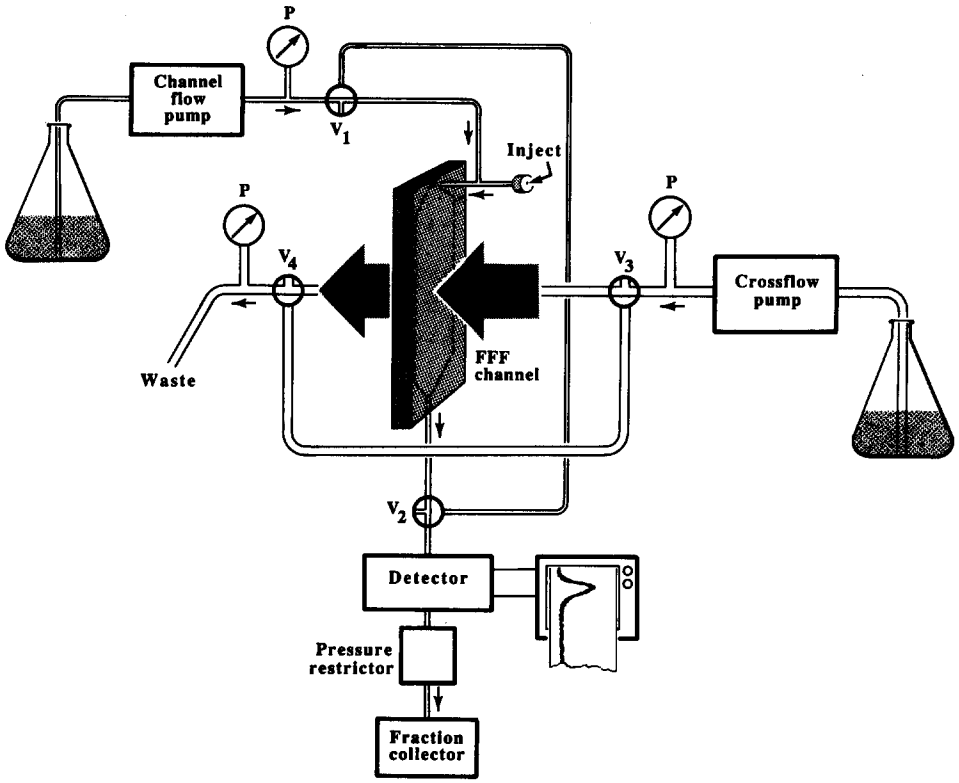

Fig. 2. Schematic diagram of a flow FFF apparatus. Flow paths are denoted by lines, the three-way valves are represented by V_1 ... V_4, and the pressure gauges are shown as P.

gauges were situated at the points indicated in Fig. 2 to monitor changes in pressure that could be indicative of obstructed flow paths.

FFF channel

The FFF channel consists of two Lucite blocks, each inset with a ceramic frit with 5-μm pores. Sandwiched between these two blocks are a Mylar spacer from which the channel volume has been cut and a 10000 molecular weight cutoff membrane (Amicon YM10, Amicon, Danvers, MA, U.S.A.). This membrane is stretched over one of the frit surfaces and serves as the accumulation wall. The opposing (depletion) wall is defined by the frit of the second block. The dimensions of the channel are 27.2 cm in tip-to-tip length, 2 cm in breadth, and 0.0254 cm in thickness. The channel was placed in a vertical position so as to avoid gravitational contributions to the crossflow field[24].

Experimental procedure

After sample is injected into the system, the channel flow is halted during the relaxation period, equal to the time that it takes to displace one channel volume through the system by the crossflow. This stopflow procedure is implemented by using

two three-way valves, V_1 and V_2, to reroute the channel flow along an external pathway. At the end of the stopflow period, V_1 and V_2 are returned to their original positions. A flow-control modification that is often used involves the addition of a crossflow loop. By connecting the inlet of the crossflow pump to the outlet of the crossflow stream (emerging from the Lucite block), the syringe pump acts as an "unpump" to withdraw a volume of liquid from the channel equal to that being pumped in. This configuration alleviates problems of flow control associated with the frequent change in lengths of tubing used as pressure restrictors on the channel flow or crossflow streams. This crossflow loop is not used at all times because of the possible contamination of the recirculated carrier due to permeation through the membrane of unknown substances present in the sample. An alternative would be to use a separate pump to withdraw the crossflow.

Reagents and samples

The carrier liquid is doubly distilled and deionized water containing 0.1% of the surfactant Fl-70 (Fisher Scientific, Fairlawn, NJ, U.S.A.) and 0.02% NaN_3, a baeteriocide. Polystyrene latex particle standards (Duke Scientific, Palo Alto, CA, U.S.A.) with nominal diameters of 19.58, 15.00, 9.87, 7.0 and 5.002 μm (hereafter 20, 15, 10, 7, and 5 μm) were used to determine the calibration parameters for the system. The identity and characteristics of the HPLC-grade silicas that were surveyed are summarized in Table I. Sample volumes of 20 μl of 5-mg/ml silica suspensions were injected directly onto the channel using a 25-μl syringe (Hamilton, Reno, NV, U.S.A.).

Electron microscopy

Electron micrographs of various fractograms were obtained using a Hitachi S-450 scanning electron microscope (Hitachi Scientific Instruments, Nissei Sangyo America, Mountain View, CA, U.S.A.). The specimens of the unfractionated samples

TABLE I

IDENTITY AND CHARACTERISTICS OF HPLC SILICA SUPPORTS SURVEYED

	Type	*Supplier*	*Batch number*	*Pore size (Å)*	*Pore volume (ml/g)*	*Surface area (m^2/g)*
Nominal 5-μm spherical silica						
a	Spherex	Phenomenex	N6052	100		180
b	Hypersil	Shandon	5-148R	120	0.61	175
c	IB-Sil	Phenomenex	5-272	110		160
d	Nucleosil	Machery-Nagel	5121	120	0.7	
e	W-Porex	Phenomenex	PR12187	100		370
f	Spherisorb	Phase Separations		80		190
Nominal 3-μm spherical silica						
g	Hypersil	Shandon	3-51	120	0.63	185
Nominal 5-μm irregular silica						
h	Maxsil	Phenomenex	7081	65		520
i	Partisil	Whatman	101801	85		350
j	LiChrosorb	EM Science	702F424488	100		420

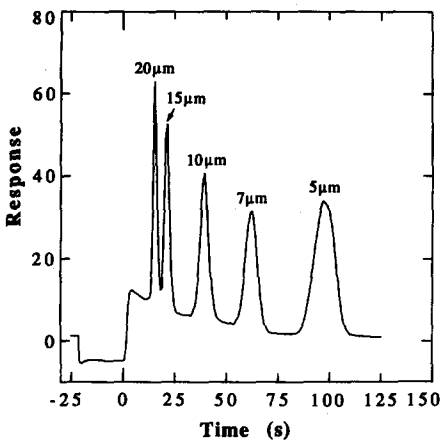

Fig. 3. Fractogram of nominal 19.58 (20)-, 15.00 (15)-, 9.87 (10)-, 7.0 (7)-, and 5.002 (5)-μm polystyrene standards. The experimental conditions were stopflow time t_{sf} = 60 s, channel flow-rate $\dot{V}$ = 6.34 ml/min, and crossflow flow-rate $\dot{V}_c$ = 2.09 ml/min. The detector was set at 254 nm and 0.02 a.u.f.s.

were prepared by filtering 0.5 ml of a 0.15-mg/ml silica suspension through a Swinney filter holder (Gelman Sciences, Ann Arbor, MI, U.S.A.). Particles were collected on a 13-mm Nuclepore membrane filter (Pleasanton, CA, U.S.A.) with 0.1-μm pores. This membrane filter was mounted on a steel stub and the filter surface was coated with gold and palladium. Typical microscope settings were 15 kV acceleration voltage with 1000 × magnification. Measurement of particle sizes could be made to within 0.05 μm with the help of a magnifier. The electron microscope was calibrated using an NBS (now National Institute of Standards and Technology) 9.89-μm polystyrene standard (SRM 1960).

RESULTS AND DISCUSSION

Preliminary experiments were carried out to determine a suitable sample concentration, specifically, one that gave a good detector response without overloading the system[25]. This was done by injecting samples of varying particle concentrations and noting changes in peak shapes and elution times. Concentrations of *ca.* 5 mg/ml of silica injected in 20-μl volumes (totaling *ca.* 100 μg of silica) gave satisfactory results and were used throughout these experiments.

The high degree of selectivity and the speed of separation attainable by flow/hyperlayer FFF is demonstrated in Fig. 3, which shows a fractogram of five polystyrene latex standards ranging from 5 to 20 μm in diameter. Baseline (or higher) resolution of all particle populations is obtained within 2 min of the start of flow (following a stopflow period of 1 min). This separation time can be significantly shortened by employing a higher axial flow-rate and/or a lower field strength. As demonstrated previously[16], the partial separtion of 49, 30, and 29-μm latex beads can be accomplished in 6 s. However, there is a loss of resolution with increasing analysis speed. Fig. 3 also confirms that the selectivity of flow/hyperlayer FFF is greater than unity. This is demonstrated by the fact that the retention time for the 5-μm latex particle is more than twice that of the 10-μm latex.

The series of fractograms shown in Fig. 4a and b were obtained for spherically and irregularly shaped HPLC silicas, respectively. Each specific packing material yields a characteristic peak shape and maximum, indicating differences in size distributions and in most cases in mean particle diameters. The size variation or polydispersity of the samples is reflected in the peak width in accordance with our earlier theoretical discussion.

In order to obtain quantitative information on particle size characteristics, a moments analysis was carried out for all the fractograms shown in Fig. 4. The first moment was used to identify the center of gravity of the peak. The retention time of the center of gravity can be converted into a mean particle diameter by means of the diameter scale shown on the upper horizontal axis of the figures. The diameter scale was obtained from the latex calibration procedure noted earlier using calibration line a from Fig. 1. The second moment was used to calculate the polydispersity or C.V. of

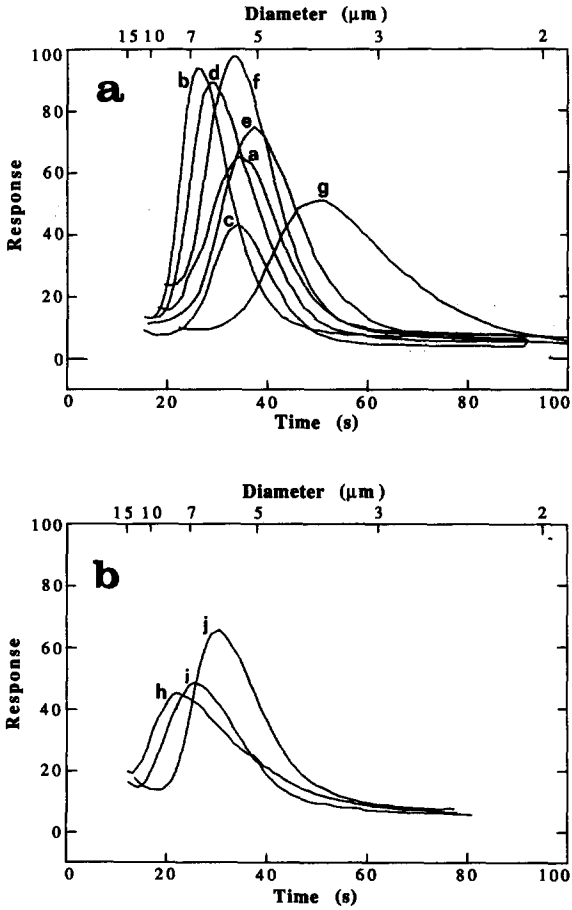

Fig. 4. Fractograms of HPLC silicas. Conditions were t_{sf} = 70 s, $\dot{V}$ = 7.55 ml/min, and $\dot{V}_c$ = 1.70 ml/min, (a) for spherical 5- and 3-μm silica and (b) for irregular 5-μm silica. The lettered fractograms correspond to silica packings from various manufacturers as listed in Table I. The diameter scale on the upper x-axis was determined using polystyrene standards.

TABLE II

SUMMARY OF THE MEAN RETENTION TIMES (t_r), DIAMETERS, AND POLYDISPERSITIES (C.V.) OF VARIOUS CHROMATOGRAPHIC SILICAS

		t_r (s)	Diameter (μm)		% C.V.
			FFF[a]	SEM	FFF[b]
Nominal 5-μm spherical particles					
a	Spherex	38.0	4.78	4.72	17.2
b	Hypersil	30.2	5.97	6.11	16.6
c	Nucleosil	36.3	5.00	5.15	15.3
d	IB-Sil	32.9	5.42	5.54	18.4
e	W-Porex	42.3	4.31	4.26	20.0
f	Spherisorb	36.9	4.87	4.94	15.1
Nominal 3-μm spherical particles					
g	Hypersil	59.0	3.19	3.29	20.5
Nominal 5-μm irregularly shaped particles					
h	Maxsil	29.7	6.21	–	22.4
i	Partisil	30.7	5.97	–	21.3
j	LiChrosorb	35.9	5.10	–	19.4

[a] Diameter calculated using the first moment of the FFF particle peak.
[b] % C.V. = $\sigma_t/(S_d t_r)$ where S_d = 1.05.

the sample by means of eqn. 10. Values of the mean diameter and the C.V. of all the samples are presented in Table II.

We note that the sample peaks shown in Fig. 4 are obtained by means of a conventional HPLC UV detector. When applied to particles, the signal from such a detector is largely generated by light scattering. The intensity of the scattered light is a complex function of particle diameter. Thus the curves in Fig. 4 cannot be precisely identified with either number distributions or mass distributions. However, the light scattering distortions for large particles are relatively small, making it likely that the peaks in Fig. 4 represent an intermediate distribution between number and mass distributions. Because the peaks are relatively narrow, the differences are less substantial than for broader distributions. The validity of this procedure for determining mean particle diameters is verified by a comparison with the results of scanning electron microscopy (SEM), also shown in Table II.

Each of the SEM diameters listed in Table II represents an average of at least 200 diameter measurements. From these measurements, the number average diameter was calculated. The maximum difference between the mean diameters obtained by FFF and SEM is 3%. Note that no SEM values are reported for the irregular particles because of the difficulty of specifying a unique diameter. The FFF diameters reported for the irregular particles in Table II are an equivalent spherical diameter.

All experiments were initially carried out with sample introduction at the top of the channel (followed by downward flow). A second series of experiments was conducted with samples injected from the bottom (followed by upward flow) to verify the results already obtained. A difference of approximately 5% was observed between the two elution time values. This discrepancy, which is not observed for polystyrene

particles, is due to gravitational effects which become more pronounced with higher density samples. The ideal (gravity-free) elution time lies between the values obtained by injection from the top and from the bottom of the channel; thus, the average of these two retention times was used to obtain the t_r in Table II.

With the exception of the small gravitational effect that is found in comparing upward and downward flow, gravity has no effect on the outcome of flow/hyperlayer FFF experiments. Thus density has no substantial role in the acquisition of particle size data. In this respect, flow/hyperlayer FFF has a definite advantage over all sedimentation-based techniques where both size and density play a role in characterization. In the latter case, particle-to-particle differences in density would lead to apparent size differences. It is possible that density as well as size variations could be examined by combining flow/hyperlayer and sedimentation/steric FFF as a multidimensional technique. However, for size data alone, unless there is some assurance of density uniformity, flow/hyperlayer FFF is advantageous.

Table II shows that the average diameters obtained for the nominal 5-μm spherical silica particles by the FFF technique range from 4.3 to almost 6.0 μm. These results are confirmed by the electron microscopy data in the table. The different support sizes reflected by these numbers will cause measurable differences in back pressure, column efficiency, and reduced plate height.

The size variations within the HPLC silicas from different suppliers, as measured by the % C.V. values, lie between 15 and 23%. The % C.V. value for 5–10-μm silica is commonly reported to be between 10 and 20%[15].

The reproducibility of the data obtained by flow/hyperlayer FFF is demonstrated in Table III. This table reports the standard deviation (S.D.) and percentage relative standard deviation (% R.S.D.) in the mean retention time t_r and in the peak

TABLE III

REPRODUCIBILITY OF THE FLOW/HYPERLAYER FFF RESULTS

	Retention time (s)			*Peak width (s)*		
	t_r[a]	*S.D.*	*% R.S.D.*	σ_t	*S.D.*	*% R.S.D.*
Nominal 5-μm spherical particles						
Spherex	37.0	0.153	0.414	6.68	0.106	1.59
Hypersil	29.4	0.577	1.96	5.12	0.187	3.65
Nucleosil	35.4	0.945	2.67	5.68	0.416	7.32
IB-Sil	32.0	0.503	1.57	6.18	0.265	4.29
W-Porex	41.2	0.153	0.371	8.66	0.254	2.93
Spherisorb	35.9	0.954	2.66	5.71	0.178	3.12
Nominal 3-μm spherical particles						
Hypersil	57.5	0.651	1.13	12.4	0.352	2.84
Nominal 5-μm irregularly shaped particles						
Maxsil	28.9	–	–	7.97	–	–
Partisil	29.9	1.58	5.28	6.69	0.361	5.40
LiChrosorb	35.0	0.543	2.86	7.13	0.135	1.89

[a] Injection from the top of the channel.

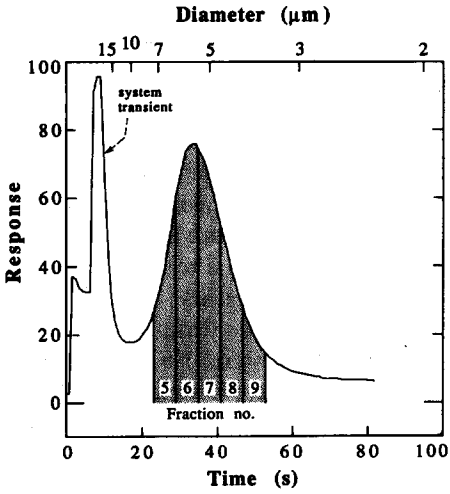

Fig. 5. Spherex 5-μm silica was characterized using the same conditions as listed in Fig. 4. Fractions of 0.76 ml were collected every 6 s starting at the time that channel flow is resumed after stopflow. The labelled fractions were examined by SEM. The observed system transients are due to pressure fluctuations in the system as the channel flow is recommenced.

width expressed as σ_t for 3–5 measurements on each sample of t_r and σ_t. The % R.S.D. in t_r and σ_t average only about 2 and 4%, respectively. The % R.S.D. in mean particle diameter and C.V. are comparable to these values.

The ability of FFF to differentiate a continuous distribution of particle sizes is demonstrated when fractions of the eluting sample are collected for further study. Silica (Spherex) was injected and the fractions collected at 6-s intervals as shown in Fig. 5. Micrographs for the original sample along with fractions 5, 7 and 9 are shown in Fig. 6. A distinct size difference can be observed among the various fractions. The results of diameter measurements made from the micrographs are summarized in Table IV. Based on the time that the cut was made, it was possible to calculate the expected diameter range of the particular fraction. The average diameters obtained from SEM measurements (based on approximately 60 particles for each sample) fall within this range for fractions 5, 6, and 7 and are only slightly higher for fractions 8 and 9. The observed trend is for smaller SEM diameters than predicted with the fractions collected on the rising slope of the peak and larger average diameters for those collected on the decreasing slope. This is as expected since there is a continuous gradient in the particle population from one edge of the cut to the other. The average particle diameter in each fraction will then be biased toward the center of the peak[23]. The C.V. of the fractions as obtained from SEM measurements for each fraction is considerably lower than that of the original sample (5–7% with the exception of fraction 5). The C.V. is, nonetheless, relatively large due to the finite volume of each cut.

It is possible to utilize the present FFF method to identify the presence of unusual and undesirable particle sizes or particle aggregates in a sample. A fractogram of a commercially available 3-μm silica packing is shown in Fig. 7. The first two peaks

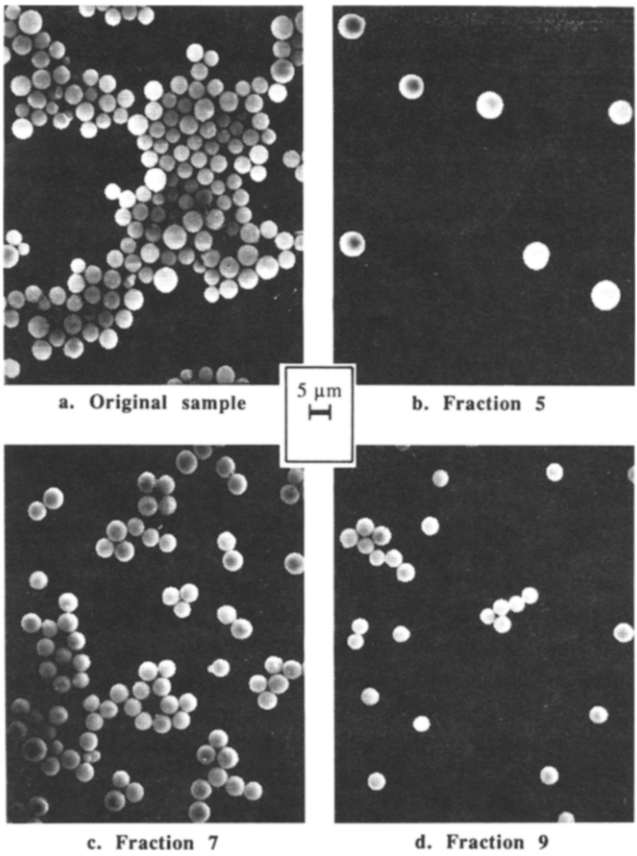

Fig. 6. Micrographs corresponding to (a) original sample, (b) fraction 5, (c) fraction 7, and (d) fraction 9 of the Spherex silica. The cut positions are depicted in Fig. 5. The micrographs were taken at 1000× magnification and at an acceleration voltage of 15 kV.

are system transients that are caused by slight changes in pressure when the channel flow is resumed at the end of the relaxation period. The presence of two sample peaks, at 13 and 56 s, suggests a bimodal size distribution. The second peak of the two

TABLE IV

COMPARISON OF EXPECTED AND ACTUAL DIAMETERS OF FRACTIONS COLLECTED FOLLOWING FRACTIONATION OF SPHEREX SILICA

Fraction number	*Time of cut (s)*	*Diameter based on time of cut (μm)*	*Diameter based on SEM (μm)*
5	24–30	7.43–6.01	6.21 ± 0.68
6	30–36	6.01–5.05	5.49 ± 0.40
7	36–42	5.05–4.36	4.86 ± 0.28
8	42–48	4.36–3.84	4.58 ± 0.29
9	48–54	3.84–3.43	4.18 ± 0.28

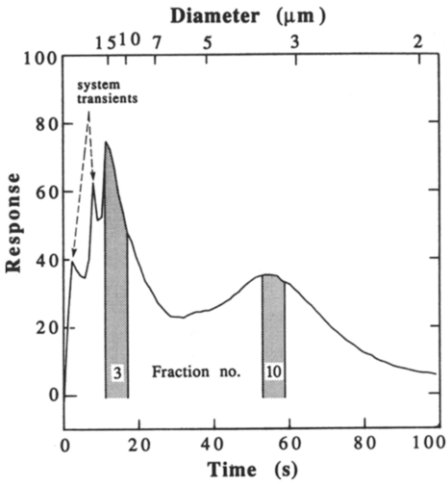

Fig. 7. Fractogram of a 3-μm commercial HPLC silica indicating the presence of anomalous large diameter components. Conditions are identical to those listed in Fig. 4.

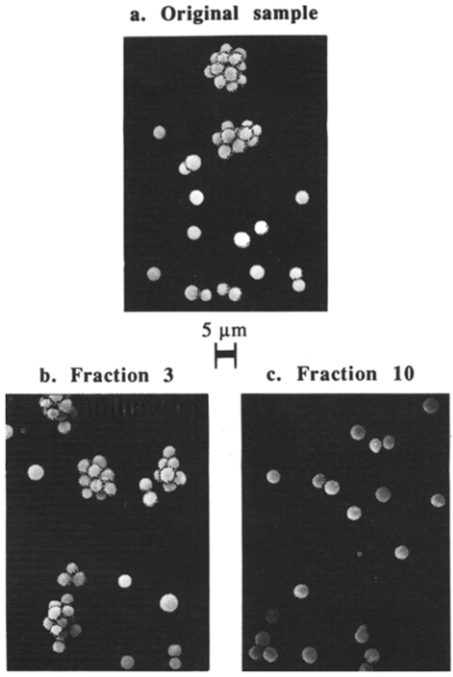

Fig. 8. Electron micrographs of the 3-μm silica whose fractogram is shown in Fig. 7. (a) Original sample, (b) fraction 3, and (c) fraction 10. SEM conditions are 15 kV acceleration voltage and 1000× magnification.

corresponds to a particle diameter of just over 3 μm as expected for this material. The first peak corresponds to a diameter of approximately 13 μm, indicating the presence of particles that obviously do not belong in the support material. These two peaks can be explained by the micrographs of Fig. 8. Fraction 3, taken from the first peak (see Fig. 7), contains aggregates whereas fraction 10, from the second peak, consists of uniform silica monomers. The micrograph of the original sample, Fig. 8a, shows a collection of aggregates and monomers of various sizes. Micrographs of the original samples taken after 20 min of sonication still showed the presence of these aggregates.

CONCLUSION

Flow/hyperlayer FFF is a rapid and reproducible technique for particle characterization. The high speed of analysis makes this technique well suited for quality control. Adjustments for any day-to-day fluctuations in the systems are easily achieved using polystyrene latex beads as internal standards. Other attractive features include the operational and instrumental simplicity of the system and the straightforward calculations of particle size and polydispersity. Flow/hyperlayer FFF has also been demonstrated as a potential tool in the preparation of small quantities of samples having narrow size distributions.

ACKNOWLEDGEMENTS

The authors would like to thank Phenomenex for contributing most of the silica packings used in this work and Shandon and Machery-Nagel for donations of samples manufactured by their respective companies. This work was supported by National Science Foundation Grant CHE-8800675.

REFERENCES

1 M. Verzele, J. Lammens and M. Van Roelenbosch, *J. Chromatogr.*, 186 (1979) 435.
2 R. Ohmacht and I. Halasz, *Chromatographia*, 14 (1981) 155.
3 R. Ohmacht and I. Halasz, *Chromatographia*, 14 (1981) 216.
4 C. Gonnet, C. Bory and G. Lachatre, *Chromatographia*, 16 (1982) 242.
5 H. Engelhardt and G. Ahr, *Chromatographia*, 14 (1981) 227.
6 J. C. Giddings, *J. Chromatogr.*, 13 (1964) 301.
7 K. D. McMurtrey and P. J. DesLauriers, *Anal. Chem.*, 55 (1983) 396.
8 K. K. Unger and M. G. Gimpel, *J. Chromatogr.*, 180 (1979) 93.
9 D. A. Hanggi and P. W. Carr, *J. Liq. Chromatogr.*, 7 (1984) 2323.
10 J. C. Giddings, M. N. Myers, K. D. Caldwell and J. W. Pav, *J. Chromatogr.*, 185 (1979) 261.
11 T. Koch and J. C. Giddings, *Anal. Chem.*, 58 (1986) 994.
12 R. Karuhn, R. D. Wood and S. D. Wyatt, *LC · GC Mag. Liq. Gas Chromatogr.*, 4 (1986) 1072.
13 B. Monaghan, Shandon Southern Products Limited, Cheshire, personal communication.
14 R. Endele, I. Halász and K. Unger, *J. Chromatogr.*, 99 (1974) 377.
15 K. K. Unger, *Porous Silica. Its Properties and Use as Support in Column Liquid Chromatography* (*J. Chromatogr. Libr.*, Vol. 16), Elsevier, Amsterdam, 1979.
16 J. C. Giddings, X. Chen, K.-G. Wahlund and M. N. Myers, *Anal. Chem.*, 59 (1987) 1957.
17 K. D. Caldwell, T. T. Nguyen, M. N. Myers and J. C. Giddings, *Sep. Sci. Technol.*, 14 (1979) 935.
18 J. C. Giddings, *Sep. Sci. Technol.*, 18 (1983) 765.
19 P. S. Williams, T. Koch and J. C. Giddings, in preparation.
20 M. N. Myers and J. Calvin Giddings, *Anal. Chem.*, 54 (1982) 2284.

21 Y. S. Gao, K. D. Caldwell, M. N. Myers and J. C. Giddings, *Macromolecules*, 18 (1985) 1272.
22 S. Lee, M. N. Myers, R. Beckett and J. C. Giddings, *Anal. Chem.*, 60 (1988) 1129.
23 J. C. Giddings and F.-S. Yang, *J. Colloid Interface Sci.*, 105 (1985) 55.
24 X. Chen, K.-G. Wahlund and J. C. Giddings, *Anal. Chem.*, 60 (1988) 362.
25 M. E. Hansen, J. C. Giddings and R. Beckett, *J. Colloid Interface Sci.*, in press.